α-Synuclein induces deficiency in clathrin-mediated endocytosis through inhibiting synaptojanin1 expression

Dong-Yan Song
Northeastern University College of Life Sciences and Health
Lin Yuan
China Medical University
Na Cui
China Medical University
Cong Feng
China Medical University
Lanxia Meng
Renmin Hospital of Wuhan University: Wuhan University Renmin Hospital
Xin-He Wang
Northeastern University College of Life Sciences and Health
Man Xiang
China Medical University
Di Liu
Northeastern University College of Life Sciences and Health
Chun Wang
China Medical University
Zhentao Zhang
Renmin Hospital of Wuhan University: Wuhan University Renmin Hospital
Jia-Yi Li
China Medical University
WEN LI (fox393933570@126.com)
China Medical University https://orcid.org/0000-0002-0383-0240

Research

Keywords: α-synuclein, Parkinson's disease, clathrin-mediated endocytosis, synaptojanin1, synaptic vesicle

Posted Date: July 13th, 2022

DOI: https://doi.org/10.21203/rs.3.rs-1843419/v1

Abstract

Background

Parkinson's disease (PD) is mainly characterized by the pathological feature of α-synuclein (α-syn) aggregation, with the exact disease pathogenesis unclear. During the onset and progression of PD, synaptic dysfunction including dysregulation of axonal transport, impaired exocytosis and endocytosis are identified as crucial events of PD pathogenesis. It has been reported that overexpression of α-syn impairs clathrin-mediated endocytosis (CME) in the synapses. However, the underlying mechanisms remained unknown.

Methods

In this study, we investigated the molecular events underlying the synaptic dysfunction induced by overexpression of wild-type human α-syn and its mutant form, involving series of proteins participating in CME.

Results

We found that excessive human α-syn causes impaired fission and uncoating of clathrin-coated vesicles (CCVs) during synaptic vesicle recycling, leading to reduced clustering of synaptic vesicles near the active zone and increased size of plasma membrane and number of endocytic intermediates. Furthermore, overexpressed human α-syn induced changes of CME associated proteins, among which synaptojanin1 (SYNJ1) showed significant reduction in various brain regions. Overexpression of SYNJ1 in the primary neuron of α-syn transgenic mice recovered the synaptic vesicle density and clustering. Using fluorescence-conjugated transferrin, we demonstrated that SYNJ1 re-boosted the CME activity by restoring the phosphatidylinositol-4,5-bisphosphate [$PI(4,5)P_2$] homeostasis.

Conclusions

In summary, our data suggested that overexpression of α-syn disrupts synaptic function through interfering with vesicle recycling, which could be alleviated by re-availing of SYNJ1. Our study unrevealed a molecular mechanism of the synaptic dysfunction in PD pathogenesis and provided a potential therapeutic target for treating PD.

Background

α-Synuclein (α-Syn) is known to be involved in the major neuropathology of Parkinson's disease (PD), forming cytoplasmic inclusions called Lewy bodies (LBs) and Lewy neurites (LNs) [1–3]. The accumulation and aggregation of α-syn have been reported to cause multiple cellular dis-homeostasis,

particularly synaptic defects at the early stages of the disease [4, 5]. Recently, mutations in synaptojanin1 (SYNJ1) [6–9], auxilin (DNAJC6) [10–12] and endophilin-A1 (SH3GL2) [13] have been identified as the risk factors in PD, all of which cause synaptic deficiency involving clathrin-mediated endocytosis (CME) [14–16].

CME is the predominant internalization route in synaptic vesicle recycling [17, 18]. Mechanistically, CME is initiated by the recruitment of clathrin by adaptor proteins such as Epsin [19], AP-2 [20] and AP180 [21], in association with phosphatidylinositol 4,5-bisphosphate [PI(4,5)P_2] lipids [22]. Thereafter, endophilin-A (EndoA) function as a membrane bender, folding the invagination of the nascent deforming vesicle [23]. Once the clathrin-coated pit (CCP) is matured, a membrane remodeling GTPase dynamin stimulates the fission of the CCP from the plasma membrane [24], together with other membrane-bending proteins, such as amphiphysin (Amp) [25] and EndoA [26, 27]. In conjunction with the fission, the phosphatase SYNJ1 dephosphorylates PI(4,5)P_2 to PI4P and PI [28, 29]. These dephosphorylations stimulate AP-2 release from the clathrin-coated vesicles (CCVs), subsequently allowing the clathrin disassembling chaperone Heat-shock cognate (Hsc70) and its cofactor auxilin to shed clathrin-coat [30, 31]. Once the CCV is uncoated, the majority of the nascent vesicles are quickly transported to synaptic vesicle pools for neurotransmitter refilling [32].

α-Syn was reported to play a role in mediating membrane curvature and tabulation [33]. Studies showed that overexpression of α-syn increased clathrin-coated vesicles along the plasma membrane, by defected vesicle fission, where PI(4,5)P_2 was significantly elevated [34–36]. PI(4,5)P_2 is a key signaling phospholipid involved in recruiting clathrin adaptors and their accessory factors to the plasma membrane [37, 38]. PI(4,5)P_2 also binds to EndoA and dynamin, contributing to the fission of endocytic vesicles [39, 40]. Importantly, PI(4,5)P_2 are inter-converted by SYNJ1 to rapidly change membrane concentration for the vesicle uncoating [41]. An elevation of steady-state PI(4,5)P_2 indicated a deficiency in SYNJ1 capacity for dephosphorylation [42]. Therefore, α-syn may interfere with CME by altering SYNJ1 expression level and distribution as an upstream effect of PI(4,5)P_2 in the cascade of CME activities.

In the present study, we aimed to elucidate the molecular mechanisms underlying aberrant α-syn-induced CME dysfunction. We employed two transgenic mouse models, i.e., mice that express BAC-α-Syn-GFP under the control of endogenous α-syn promotor and that express human α-syn-A53T under the control of PrP promotor, respectively, through electron microscopy (EM) and analyses of the cascade interactions of CME proteins, we observed the selective impairment of CCV uncoating and fission induced by α-syn, leading to expansion of the plasma membrane and diffused SV distribution. CME-associated proteins, such as SYNJ1, predominantly decreased in α-syn transgenic mice, while knock-down of α-syn expression normalized the CME-related protein levels. Furthermore, we found that both the expression level and distribution of SYNJ1 altered, with clustered pattern in the cytosol. Overexpression of SYNJ1 normalized the aberrations by elevating synaptic vesicle clustering and enriching the density of dendritic vesicles. Finally, using fluorescence-conjugated transferrin, we demonstrated that SYNJ1 attenuates CME activity

by retrieving $PI(4,5)P_2$ homeostasis. Our results showed that SYNJ1 is a key modulator of CME activity upon α-syn pathology, which may present a valuable therapeutic target in the early prevention of PD.

Materials And Methods

Animals

The BAC-α-syn-GFP mice were generated as previously reported [43]. Briefly, recombinant BAC (Bacterial Artificial Chromosome) DNA consisting the full-length human wild-type (WT) α-syn gene fused with green fluorescent protein (GFP) consisted was inoculated into the pronuclei of C57BL/6J fertilized eggs (Jackson Laboratories, Bar Harbor, ME, USA). The BAC-α-syn-GFP mice overexpress WT human α-syn driven by mouse α-syn promoter. BAC-α-syn-GFP, C57BL/6J and α-syn-A53T mice (Jackson Laboratories, Bar Harbor, ME, USA) were randomly assigned to different groups and housed five to six per cage under a 12-h light-dark cycle with food and water *ad libitum*. All animal experimental procedures were approved by the Ethical Committees for use of laboratory animals at Lund University, Sweden, and at Northeastern University, China.

AAV virus and plasmid construct

The vector for production of AAV2 ITR including shRNA of human WT α-syn-AcGFP, driven by U6 promoter and enhanced using a mCherry which was driven by CMV promoter, were produced by Brain VTA (Wuhan, China). The Flag-His-SYNJ1 plasmids encoding full-length SYNJ1 with the human synapsin I promoter and EGFP/3xFlag-tag were described previously [44].

Tissue preparation

Mice (n = 3–5 in each group) were deeply anesthetized with sodium pentobarbital and perfused with 0.9% sodium chloride (NaCl) transcardially. Hippocampal and striatal tissues for protein analyses were rapidly collected and snap frozen in liquid nitrogen. For immunohistochemistry, brains were perfused with 4% paraformaldehyde (PFA) for 10 min and then dissected, post-fixed in 4% PFA overnight and transferred to gradient sucrose solution in 0.1 M phosphate buffered saline (PBS). Thirty μm thick free-floating sections were cut on a microtome (Leica, SM2010R, Wetzlar, Germany).

Stereotactic injection of the AAV viruses

rAAV6-U6-shRNA1 (α-syn-AcGFP) vectors were used for inducing the knock-down (KD) of human WT-α-syn-GFP in BAC mice, with empty vectors as contralateral controls. After general anesthesia with 50 mg/kg sodium pentobarbital, rAAV6-U6-shRNA1 (α-syn-AcGFP) were injected into the right dorsal dentate gyrus (DG) (Coordinates: 1.8 mm posterior to bregma, 1.2 mm lateral from midline and 1.65 mm dorsoventral from the dura). α-syn-AcGFP empty vectors were delivered to the corresponding left dorsal DG of mice. Each injection was performed with 15 min duration and the micropipette was left in the injection site for an additional 5 min. Mice were sacrificed 6 weeks post-viral delivery.

Western blot analyses

Hippocampal and striatal tissues were fully immersed in ice-cold radioimmunoprecipitation assay lysis buffer (Beyotime, Cat. #P0013B, Shanghai, China) containing 2 mM PMSF (Beyotime, Cat. #ST505, Shanghai, China), 1% protease inhibitor cocktail (Seven, Cat. #SW105-02, Beijing, China) and 1% phosphatase inhibitor cocktail (Bimake, Cat. #B15001, HOU, USA), homogenized by ultrasonic crashing and incubated at 4 ◦C for 1 h. After centrifugation at 13000rpm for 30 min, proteins were collected from supernatants and the concentrations were measured using BCA kit (TransGen Biotech, Cat. #DQ111-01, Beijing, China). Before loading onto gels, proteins were diluted in 5X SDS (Solarbio, Cat. #P1040, Beijing, China) loading buffer and boiled 5 min at 95 ◦C. The sample was loaded, 20 μg per lane and 10% SDS-PAGE was run first at 80 V, 120 min followed by 120 V, 70 min before transferred onto poly-vinylidene difluoride membranes (Millipore, Cat. #IPVH00010, MA, USA). Membranes were blocked with 5% skim milk solution (BD, Cat. #232100, USNJ, USA) in Tris-buffered saline (TBS) with 0.1% Triton X-100 at room temperature (RT) for 1 h. Primary antibody incubations (Additional file 1: Table S1) were performed overnight at 4°C in TBS. After washing, horseradish peroxidase (HRP)-labeled secondary antibodies (Additional file 1: Table S1) were applied at RT for 1 h. The membranes were developed using enhanced chemiluminescence (ECL) Kits (Tanon, Cat. #180–5001, Shanghai, China) and imaged using chemiluminescence imaging analysis system (Tanon, 5500, Shanghai, China). Fiji 1.0 (National Institutes of Health, MD, USA) was used to quantify the intensity of the bands corresponding to the related proteins.

Electron microscopy

CA1 region of hippocampus of 14-month-old WT mice, BAC-α-syn-GFP mice and α-syn-A53T mice were dissected into 1 mm^3 cubes and post-fixed with 2.5% glutaraldehyde in PBS at 4°C overnight. Seventy nm ultrathin sections were cut and mounted onto carbon-coated grids, observed with a transmission electron microscope (Hitachi, H-7650, TKY, Japan). Seventy to one hundred images with synapses were taken at a fixed magnification (50,000 ×) per group from n = 3 animals. The synapses were identified by the presence of both the pre-synaptic element containing vesicles and the post-synaptic electron-density. Vesicles were quantified every 500 nm radius within each presynaptic active zone, including number and density of SVs, extent of plasma membrane (PM) evaginations, number of membranous “cisternae”, and total number and stage of CCPs and CCVs per terminal.

Immunohistochemistry and immunocytochemistry

Free-floating sections were antigen-retrieved in 0.1 M citrate acid buffer (pH = 6) at 70°C for 40 min, quenched by 3% hydrogen peroxide in methanol at RT for 15 min, and blocked in 10% normal goat serum and 0.3% Triton X-100 in 0.1 M PBS at RT for 1 h. Primary antibody incubation (Additional file 1: Table S1) was performed at 4°C overnight, followed by secondary antibody incubation (Additional file 1: Table S1) at RT for 2 h. Standard ABC (Vector Laboratories, Cat. #PK-6100, CA, USA) kit was then applied at RT for 1 h before developing with DAB (Vector Laboratories, Cat. #SK-4100, CA, USA). Sections were dehydrated with rising gradience of ethanol before mounted with neutral balsam (Meilunbio, Cat. #MB9899, Dalian, China). Images were acquired using a microscope (Nikon, Eclipse Ni-E/Ni-U, TKY, Japan).

Cells were fixed with 4% PFA at RT for 20 min, permeabilized with 0.25% Triton X-100 in PBS for 10 min and washed. Blocking was applied with 10% normal goat serum in PBS for 1 h and primary antibody incubation (Additional file 1: Table S1) was performed at 4°C overnight, followed by secondary antibody incubation (Additional file 1: Table S1) at RT for 1 h. After washing cells were mounted in anti-fluorescence quenching sealing reagent (Beyotime, Cat. #P0126, Shanghai, China). Fluorescent images were taken using a confocal laser scanning system (Nikon, X-Light V3, TKY, Japan).

Primary neuronal culture and transfection

Primary neuronal cultures were prepared from the hippocampus of neonatal mice. Hippocampal neurons were dissected and cultured as previously described [45]. Briefly, the hippocampus was extracted and digested in trypsin (Sigma, Cat. #T8154, SL, USA). After manual trituration, single cells were plated onto coverslips coated with 0.5 mg/ml poly-L-lysine (Thermo, Cat. #15400054, MA, USA) at a density of 30,000 cells/cm^2 in plating medium, DMEM (Gibco, Cat. #C12430500BT, Shanghai, China) with 3% horse serum (Gibco, Cat. #16050-130, New Zealand), 2% B-27 supplement (Gibco, Cat. #17504-044, CA, USA) and 1% L-glutamine (Gibco, Cat. #25030081, Paisley, UK). Three to six hours after plating, the medium was changed to culture medium, Neurobasal (Gibco, Cat. #25030081, Paisley, UK) with 2% B-27 supplement and 1% L-glutamine. Neurons were maintained at 37°C in a 5% CO2 humidified incubator (Thermo, BB150, MA, USA), with partial medium change (50%) every two days. Flag-His-SYNJ1 were performed using calcium phosphate for 90 mins at 14 days *in vitro* (DIV), before subjected to imaging and staining process.

Transferrin uptake assay

Four days after Flag-His-SYNJ1 transfection, neurons were starved for 60 min in media lacking B27 supplementation at 37°C. Neurons were then treated with 25 μg/ml Alexa Fluor 647-conjugated transferrin (647-Tf) (Bioss, Beijing, China) at 37°C for 30 min, before subjected to immunocytochemistry.

Quantification

Vesicle quantification in EM

Synaptic vesicles (SVs) were defined as clear-edge round vesicles < 100 nm in diameter. CCP/Vs contained electron-dense coat around the vesicle membrane, staging as: 1-initial clathrin coated bud; 2-invaginated CCP without constricted neck; 3-invaginated CCP with constricted neck; 4-free CCV [46]. Cisternae were defined as atypical vesicles with intracellular membranous structures larger than 100 nm in diameter [47]. The total amount of membrane within individual cisternae per synapse was defined as “Total cisternae”. PM evaginations were measured as previously described be Morgan et al [48].

SV2 and SYNJ1 and $PI(4,5)P_2$ quantification

Synaptic vesicle glycoprotein 2 (SV2), which labels presynaptic vesicle clusters, and SYNJ1 puncta area and density were manually counted in Z-stack images using FIJI 1.0. Each fluorescent dot were identified as one positive puncta. The average number of SYNJ1 puncta per synaptic vesicle clusters was also

calculated. In addition, the mean fluorescence intensity of $PI(4,5)P_2$ and internalized transferrin in each phenotype were calculated by using FIJI software.

Statistical analyses

Statistical analyses were performed using GraphPad Prism 8.0 (GraphPad Software, CA, USA). All data shown were based on at least three independent experiments unless otherwise stated, presented with the mean ± standard deviation (SD). Student's *t*-tests were used to analyze differences between α-syn overexpression transgenic mice and WT mice. Two-way ANOVA with Tukey's multiple comparisons post hoc tests were used to analyze differences between α-syn overexpression transgenic mice and WT mice at different ages. To analyze the data of EM and cell experiments, we used non-parametric Kruskal Wallis test, Student's *t*-tests, as well as one or two way ANOVA when appropriate. Results with $p < 0.05$ was considered statistically significant.

Results

Available evidence has shown that overexpression of human WT-α-syn [43, 49] or mutant forms [50, 51] can lead to multi-features of pathological alterations, such as protein aggregation, protein phosphorylation, neuroinflammation, and even neuronal cell death [52]. Here, we reported that two α-syn overexpression transgenic mice, i.e., BAC-α-syn-GFP mice (called as BAC-α-syn mice below) and α-syn-A53T mice (called as α-syn-A53T mice below) exhibited impaired synaptic vesicle recycling, particularly on CME.

Alterations of CME-associated proteins in α-syn overexpressing mice

To explore the potential impacts on synaptic function in the BAC-α-syn and α-syn-A53T mice, we examined the proteins regulating synaptic vesicle endocytosis. We observed a marked decrease in proteins regulating CME processes, particularly SYNJ1 in the hippocampus and the striatum (Fig. 1, Fig. 2). We analyzed the expression levels of key CME-associated proteins in the BAC-α-syn mice at different ages. SYNJ1 appeared significantly decreased in the hippocampus (Fig. 1a, b) at 6 months of age and in the striatum (Fig. 2a, b) at 10 months of age, implying a potential impairment of CCV fission and uncoating. Auxilin, also related to CCV uncoating, decreased significantly in the hippocampus (Fig. 1c) at 14 months and in the striatum (Fig. 2c) at 10 months of age. The protein expression changes align with abundant free CCVs observed in EM. Furthermore, the clathrin heavy chain (CHC) also significantly decreased in the hippocampus (Fig. 1d) at 14 months and in the striatum (Fig. 2d) at 10 months, which may trap clathrin coats in CCVs due to impaired uncoating. The clathrin light chain (CLC) expression level remained unchanged (Fig. 1e, Fig. 2e). Moreover, Amp was also reduced in the transgenic mice at 14 months of age in the hippocampus and striatum (Fig. 1f, Fig. 2f), which may result from halted recruitment to plasma membranes due to decreased clathrin availability. In contrast, AP180 expression increased in the hippocampus and striatum (Fig. 1g, Fig. 2g) at 14 months, possibly due to a

compensatory effect. Other endocytic proteins, such as EndoA, dynamin, and Hsc70 remained unchanged (Fig. 1h-j, Fig. 2h-j).

In order to validate the findings in BAC-α-syn mice, we further examined transgenic mice overexpressing human α-syn with A53T point mutation. In the 14-month-old α-syn-A53T mice, we observed similar protein expression patterns to the BAC-α-syn mice. SYNJ1, auxilin, CHC, Amp and EndoA decreased in both hippocampus and striatum (Additional file 1: Fig. S1a-f, Fig. S2a-f), while CLC and dynamin reduced in the striatum (Additional file 1: Fig. S2g, h). Similarly, AP180 increased in the hippocampus and striatum of α-syn-A53T mice (Additional file 1: Fig. S1f, Fig. S2f).

Clustering of SYNJ1 in α-syn overexpression mice

The biochemical analyses revealed the significant reduction of SYNJ1. We then further performed immunohistochemistry to assess the pattern and distribution of SYNJ1. Compared to WT mice, marked clustering of SYNJ1, shown as differently sized patches, was observed in the hippocampus and striatum of BAC-α-syn mice from 6 months of age and became more robust with age (Fig. 3). Similar phenomena also appeared in the hippocampus and striatum in α-syn-A53T mice (Additional file 1: Fig. S3).

To determine the distribution of SYNJ1 and the effects on synaptic vesicle recycling, we further performed immunocytochemical studies with synaptic vesicle cluster marker protein SV2 and SYNJ1 in primary hippocampal neuron cultures (Fig. 4a). We compared cultured hippocampal neurons from neonatal BAC-α-syn mice and WT mice (Fig. 4b). At 18 days in culture (DIV 18), we observed the SV2 positive synaptic boutons appeared smaller in size and more sparse in the distribution in α-syn-expressing neurons, compared to WT ones, implying a diminished synaptic vesicle clustering (Fig. 4b, c). In detailed analyses with high-power images (Fig. 4c), we quantitatively analyzed the mean puncta size and density of SV2-positive and SYNJ1-positive boutons associated with dendritic profiles. We found that although SV2 positive puncta appeared in smaller in size and more sparse in density in α-syn-expressing neurons compared to WT ones (Fig. 4d, e), SYNJ1-positive profiles significantly increased in α-syn-expressing neurons compared to the WT ones (Fig. 4f). However, the density of SYNJ1 positive boutons was decreased in α-syn-expressing neurons (Fig. 4g). We hypothesized that α-syn overexpression induced CME dysfunction causes impaired neural plasticity and then causes reduced synapses, furthermore, reduced SYNJ1 availability, which are consistent with the decreased density of SV2-positive and SYNJ1-positive boutons (Fig. 4f, g). Moreover, because of the expanded plasma membrane caused by overexpressed α-syn, the SYNJ1 on the plasma membrane of α-syn-expressing neurons formed clustered aggregation, which is consistent with the increased area of each SYNJ1 puncta (Fig. 4f). Finally, double immunofluorescence labeling exhibited that the number of SYNJ1-positive boutons overlapped with SV2-positive ones significantly decreased in α-syn-expressing neurons compared to the WT ones (Fig. 4h). The data indicates that overexpression of α-syn led to reduced SYNJ1 availability during CCV uncoating.

Ultrastructural alterations of presynaptic compartments in α-syn overexpression transgenic mice

Upon the reduced to depleted key proteins regulating different steps of endocytosis, such as clathrin coating and de-coating and retrieved membrane fission from the plasma membrane, we reasoned that we may expect to detect the related deficits in ultrastructural and functional studies. To address these issues, we first performed detailed ultrastructural analyses on presynaptic membranes of BAC-α-syn and α-syn-A53T mice compared to that of WT mice (Fig. 5a-e). Compared to WT mice, expanded plasma membrane and cisternae of accumulation in the two α-syn transgenic mice (Fig. 5f). The total number of SVs remained unchanged in BAC-α-syn mice, while it significantly decreased in the α-syn-A53T mice (Fig. 5g). In the active zone, the synaptic vesicle clusters were more dispersed in the two α-syn transgenic mice than that in WT mice (Fig. 5h) and located further away from the active zone, distributed in the axoplasm (Fig. 5k). Presynaptic membranes of the two α-syn transgenic mice exhibited increased numbers of large atypical cisternae (> 100nm diameter) (Fig. 5i) and abundant clathrin-coated (CCPs + CCVs) structures (Fig. 5j), supporting that α-syn is associated to the impairment of synaptic vesicle recycling via inhibition of CME.

We calculated the number of CCPs (Stage 1–3) and CCVs (Stage 4) at presynaptic membranes among the three groups of mice. In BAC-α-syn mice, the number of free CCVs (Stage 4) increased due to the impaired uncoating step (Fig. 5l). In α-syn-A53T mice, the number of Stage 3 CCPs and Stage 4 CCVs increased, suggesting an impairment in vesicle fission and uncoating (Fig. 5l). In summary, the data reinforces the observations that overexpression of WT-α-syn and mutant (A53T) α-syn could induce disordered synaptic vesicle recycling via inhibition of CME, especially at the site of vesicle fission and uncoating.

Knock-down α-syn overexpression rescues impaired CME

In order to validate that impaired CME processes are directly contributed by overexpression of α-syn in the BAC-α-syn mice, we have designed AAV vectors to knock-down α-syn expression in this BAC-α-syn-GFP transgenic mice. The AAV vector was stereostactically injected into the hippocampus (Fig. 6a, b). Six weeks post-AAV delivery, we observed a significant reduction of α-syn-GFP and phosphorylated α-syn in the hippocampus of AAV-shRNA (α-syn-AcGFP) injected side (Fig. 6c, d). Concomitantly, we detected increased SYNJ1, CHC, and auxlin in the hippocampus of AAV-shRNA (α-syn-AcGFP) injected side compared to the contralateral side (Fig. 6e-g). Taken together, the data indicates that overexpressed α-syn impairs CME processes by inducing the decrease to depletion of different CME-associated proteins, particularly SYNJ1, targeting the fission and uncoating process. Knock-down of α-syn transgenic expression in the mice largely normalized the dysfunctioned CME processes.

Overexpression of SYNJ1 attenuates the levels of synaptic vesicle cluster and CME defects

As SYNJ1 was the most robustly changed CME protein in the α-syn expressing mice and also in the KD experiments mentioned above, we then further determined the role of SYNJ1 in α-syn-induced CME processes, we have over-expressed SYNJ1, tagged with Flag-His, in the primary hippocampal neurons

from BAC-α-syn mice or WT mice (Fig. 7a, b). We observed that, upon overexpression of SYNJ1, size and density of SV2-positive puncta associated with dendrites and dendritic spines significantly increased in α-syn-expressing (BAC-α-syn) neurons, which largely normalized the reduced SYNJ1 in the control condition (i.e. α-syn-overexpression condition) (Fig. 7c-e). Interestingly, overexpression of Flag-His-SYNJ1 did not affect WT neurons (Fig. 7c-e). This data suggests that replenishment of SYNJ1 can restore the levels of synaptic vesicle clusters, initially reduced due to overexpression of α-syn.

In order to further determine the rescuing effects of SYNJ1 on CME, we applied assays measuring transferrin endocytosis (Fig. 8a). 647-Tf uptake was significantly decreased in primary neurons of BAC-α-syn mice compared to the neurons from the WT mice (Fig. 8b, c). However, upon SYNJ1 overexpression, 647-Tf endocytosis increased markedly to the level comparable to the one of WT neurons (Fig. 8d), further strengthening that capacity of CME is largely rescued by SYNJ1 overexpression to the neurons that possess impaired CME, induced by α-syn overexpression.

SYNJ1 overexpression retrieved CME function through reducing $PI(4,5)P_2$

Previous evidence has shown that α-syn is associated with $PI(4,5)P_2$ on the plasma membrane during endocytosis, which is dephosphorylated by SYNJ1 [36]. We, therefore, examined the level of $PI(4,5)P_2$ upon SYNJ1 overexpression with the same experimental paradigm as Fig. 7 to investigate the mechanism underlying the rescuing effects of SYNJ1 on impaired CME. The average fluorescence intensity of BAC-α-syn neurons was elevated compared to WT ones (Fig. 9a, b), indicating the $PI(4,5)P_2$ dis-homeostasis induced by α-syn overexpression. However, after transduced with SYNJ1, the $PI(4,5)P_2$ levels were restored to the one of WT neurons (Fig. 9c), indicating the mediating role of $PI(4,5)P_2$ in α-syn induced CME dysfunction.

Discussion

Previous studies have shown that the endocytic function at cultured hippocampal synapses [53], lamprey nerve terminals [47] and calyces of held [54] were inhibited by normal and mutant α-syn. However, the detailed mechanisms behind are still obscure. Thus, in this work we used BAC-α-syn mice and α-syn-A53T mice to better understand how age-dependent α-syn pathology at synapses impact the pathogenesis of PD. In the two strains of α-syn overexpression transgenic mice, we observed dispersed synaptic vesicle clusters, expanded plasma membrane, increased cisternae and diminution of CME associated proteins, which suggest that excessive WT-α-syn and A53T-α-syn induce a specific defect in the synaptic vesicle recycling pathway by preventing the re-clustering of vesicles after endocytosis.

Different severity of synaptic toxicity induced by WT- and A53T-α-syn

In the present study, we observed differences in the two strains of mice regarding CCV deficiency, with WT-α-syn inhibiting CCV uncoating and A53T-α-syn inhibiting both CCV fission and uncoating. Furthermore, A53T-α-syn caused more severe plasma membrane expansion. The different synaptic toxicity between the BAC-α-syn and α-syn-A53T mice was intriguing, we reasoned that following factors may be involved. Firstly, different transgene expression in the two transgenic strains, one strain of mice express human WT α-syn, while the other express the mutated form, A53T-α-syn. Available evidence showed that α-syn-A53T mice developed more severe and earlier neurodegeneration [52, 55]. By 8 months of age, transgenic mice expressing A53T-α-syn developed an age-dependent motor impairment and α-syn inclusions in the somatodendritic compartment and dystrophic neurites, while mice expressing WT-α-syn developed aberrant α-syn accumulations or neurological defects from at least 14 months of age [50]. Moreover, it has been shown by of Rocha et al that WT-α-syn and A53T-α-syn aggregates possess different rates of interconversion and structural variants of aggregation intermediate [56, 57]. A53T-α-syn oligomerizes and forms into fibrils more rapidly and show higher potency regarding propagation and cytotoxicity to neurons than that of WT-α-syn mice [58–60].

The different synaptic toxicity of WT-α-syn and A53T-α-syn raises the question of whether strain variance play a role in neuronal toxicity of α-syn in the early phase of disease onset, as previous studies have demonstrated the structural difference between WT-α-syn aggregates and A53T-α-syn fibrils [61, 62]. It will be meaningful and important in future experiments to investigate the impacts of different α-syn conformers on CME dysfunction and to identify common mechanisms of α-syn induced synaptic deficiencies.

SYNJ1, the driving force of CME impairment in α-syn-expressing mice

The most robust evidence in the present study is reduction to depletion of SYNJ1 in response to overexpression of WT- and A53T-α-syn. SYNJ1 acts as a phosphoinositide phosphatase, through dephosphorylating $PI(4,5)P_2$ to promote dynamin-mediated membrane fission and concomitant vesicle uncoating mediated by the auxilin-Hsc70 complex [63]. Thus, we hypothesize that α-syn influence the CME and further synaptic vesicle recycling through impairment of SYNJ1 function. We discovered dispersed synaptic cluster, accumulation of CCV, expanded plasma membrane and, decreased transferrin endocytosis, which could explain for the clustered pattern of SYNJ1, in the overexpression of WT- or A53T-α-syn mice. These concomitant alterations induced by decreased SYNJ1 were consistent to previous observations in SYNJ1 ablated mice [64], worms [65], and flies [66]. Furthermore, overexpression of SYNJ1 recovered SV density and increased transferrin uptake, which were impaired by overexpressed α-syn. Our work strengthens the notion that SYNJ1 is vital in fission and uncoating function in pathological process of PD. The data presents a viable strategy by increasing SYNJ1 availability and function to stabilize the CCV uncoating for halting and even reversing neurodegeneration in PD and other synucleinopathies. Moreover, to our knowledge, the current study work is the first report, demonstrating SYNJ1 decreased in a chronic overexpression α-syn mouse model and providing evidence for a correlation between SYNJ1 and α-syn.

How the cascades of synaptic protein changes may lead to CME deficiency

How does the α-syn disturb the SYNJ1 availability and function? $PI(4,5)P_2$. $PI(4,5)P_2$ plays a vital role in the process of membrane recruitment of presynaptic proteins, especially SYNJ1 [67]. In the present study it is evident that α-syn pathology disturbed $PI(4,5)P_2$ steady-state on the plasma membrane. $PI(4,5)P_2$ dys-homeostasis leads to inhibition of the SYNJ1 recruitment and then decreased SYNJ1 conversely aggravates $PI(4,5)P_2$ dys-homeostasis, which make $PI(4,5)P_2$ failed to be transformed insufficiently to PI(3)P and $PI(3,4)P_2$. The insufficient PI(3)P and $PI(3,4)P_2$ inhibit the auxilin recruited to clathrin-coated pits and then vesicle uncoating is inhibited by the decreased auxilin-Hsc70 complex, which also cause clathrin trapped in the accumulated CCV [67]. Furthermore, the CCV accumulation influences the vesicle transported to the recycling pool. The disturbed $PI(4,5)P_2$ level and insufficient vesicle recycling pool may influence the SNARE complex synthesis and induce defective exo-endocytotic coupling process, leading to AP180 accumulation on plasma membrane, forming a trend of increase of the protein due to compensating mechanisms [68]. Our study has therefore paved out a theoretical process on how α-syn pathology induced CME dysfunction through altering cascades of protein expressions.

Conclusion

In conclusion, we have shown that SYNJ1 is the key protein in alleviating disrupted synaptic function caused by α-syn through interfering with vesicle recycling. Overexpression of SYNJ1 can restore the extent of synaptic vesicle cluster and 647-Tf endocytosis. Moreover, we have demonstrated that SYNJ1 attenuating CME activity is mediated by $PI(4,5)P_2$ homeostasis simultaneously. Thus, maintenance of normal endocytic processes requires an adequate concentration of SYNJ1. Overall, our study identified the molecular mechanisms underlying α-syn-induced CME dysfunction and provided a potential therapeutic target for treating PD.

Abbreviations

α-syn	α-synuclein	KD	knock-down
Amp	amphiphysin	LBs	Lewy bodies
BAC	Bacterial Artificial Chromosome	LNs	Lewy neurites
CCP	clathrin-coated pit	NaCl	sodium chloride
CCVs	clathrin-coated vesicles	PBS	phosphate buffered saline
CHC	clathrin heavy chain	PD	Parkinson's disease
CLC	clathrin light chain	PFA	paraformaldehyde
CME	clathrin-mediated endocytosis	$PI(4,5)P_2$	phosphatidylinositol-4,5-bisphosphate
DG	dentate gyrus	PM	plasma membrane
DIV	days *in vitro*	PSD	post-synaptic density
ECL	enhanced chemiluminescence	RT	room temperature
EM	electron microscopy	SD	standard deviation
EndoA	endophilin-A	SVs	synaptic vesicles
GFP	green fluorescent protein	SV2	synaptic vesicle glycoprotein 2
hα-syn	human α-synuclein	SYNJ1	synaptojanin1
HRP	horseradish peroxidase	TBS	Tris-buffered saline
Hsc70	Heat-shock cognate	WB	western blot
ICC	immunocytochemistry	WT	wild-type
IHC	immunohistochemistry	647-Tf	Alexa Fluor 647-conjugated transferrin

Declarations

Acknowledgements

We thank Jia-Bin Li and Chen Liu for the help of electron microscopy assay. We thank Xiao-Yan Gao, Hao-Wen Dou, Qian Wang, Yi-Qing Lv, Zhang-Li Wang, Duo Xu, Kai-Dong Zhao, Ting-Ting Huang, Dei-Hai Gou, Jian-Jun Guo, Qian-Qian Chen, Sheng Yang, for their technical supports. We thank Hui-Ling Gao and all membranes of Li's laboratory for their intellectual inputs.

Authors' contributions

DYS, WL and JYL designed research. DYS, NC, XHW performed research. DYS analyzed and interpreted the data. DYS, NC and MX designed the technology roadmap. LXM and ZTZ provided FLAG-His-SYNJ1

plasmids. LY, CF and CW provided intellectual inputs. DYS, CF, LY, WL and JYL wrote the manuscript. All authors edited and approved the final manuscript.

Funding

This work was supported by grants from National Natural Science Foundation of China (No. 81430025, 31800898, C-0054 and U1801681to JYL and WL) and the Key Field Research Development Program of Guangdong Province (2018B030337001). The Swedish Research Council (2019-01551), EU-JPND research (αSynProtec and REfrAME) and EU-Horizon2020 (MSCA-ITN-2016, SynDeGen), ParkinsonFonden, the Strategic Research Area Multipark (Multidisciplinary research in Parkinson's disease at Lund University), Hjärnfoden (PS2018-0062) and Svenska Sällskapet för Medicinsk Forskning (SSMF, P18-0194).

Availability of data and materials

All data generated or analyzed during this study are included in this published article (and its supplementary information files).

Ethics approval and consent to participate

All the work involving animals were approved by the Ethical Committees for the use of laboratory animals at Lund University, Sweden, China Medical University, China and at Northeastern University, China.

Consent for publication

All authors have read the manuscript and indicated consent for publication.

Competing interests

The authors declare that they have no competing interests.

Authors' information

[1] Institute of Neuroscience, College of Life and Health Sciences, Northeastern University, Shenyang 110169, China. [2] Laboratory of Research in Parkinson's Disease and Related Disorders, Health Sciences Institute, China Medical University, Shenyang 110122, China.[3] Department of Neurology, Renmin Hospital of Wuhan University, Wuhan 430060, China. [4] Neural Plasticity and Repair Unit, Department of Experimental Medical Sciences, Lund University, 221 84 Lund, Sweden.

References

1. Goedert M, Jakes R, Spillantini MG. The synucleinopathies: twenty years on. J Parkinsons Dis. 2017;7:51–69.
2. Lang AE, Lozano AM. Parkinson's disease. First of two parts. N Engl J Med. 1998;339:1044–53.

3. Lang AE, Lozano AM. Parkinson's disease. Second of two parts. N Engl J Med. 1998;339:1130–43.
4. Nguyen M, Wong YC, Ysselstein D, Severino A, Krainc D. Synaptic, mitochondrial, and lysosomal dysfunction in Parkinson's disease. Trends Neurosci. 2019;42:140–9.
5. Volpicelli-Daley LA, Luk KC, Patel TP, Tanik SA, Riddle DM, Stieber A, et al. Exogenous α-synuclein fibrils induce Lewy body pathology leading to synaptic dysfunction and neuron death. Neuron. 2011;72:57–71.
6. Kirola L, Behari M, Shishir C, Thelma BK. Identification of a novel homozygous mutation Arg459Pro in SYNJ1 gene of an Indian family with autosomal recessive juvenile Parkinsonism. Parkinsonism Relat Disord. 2016;31:124–8.
7. Krebs CE, Karkheiran S, Powell JC, Cao M, Makarov V, Darvish H, et al. The Sac1 domain of SYNJ1 identified mutated in a family with early-onset progressive Parkinsonism with generalized seizures. Hum Mutat. 2013;34:1200–7.
8. Olgiati S, De Rosa A, Quadri M, Criscuolo C, Breedveld GJ, Picillo M, et al. PARK20 caused by SYNJ1 homozygous Arg258Gln mutation in a new Italian family. Neurogenetics. 2014;15:183–8.
9. Quadri M, Fang M, Picillo M, Olgiati S, Breedveld GJ, Graafland J, et al. Mutation in the SYNJ1 gene associated with autosomal recessive, early-onset Parkinsonism. Hum Mutat. 2013;34:1208–15.
10. Edvardson S, Cinnamon Y, Ta-Shma A, Shaag A, Yim YI, Zenvirt S, et al. A deleterious mutation in DNAJC6 encoding the neuronal-specific clathrin-uncoating co-chaperone auxilin, is associated with juvenile parkinsonism. PLoS ONE. 2012;7:e36458.
11. Köroğlu Ç, Baysal L, Cetinkaya M, Karasoy H, Tolun A. DNAJC6 is responsible for juvenile parkinsonism with phenotypic variability. Parkinsonism Relat Disord. 2013;19:320–4.
12. Olgiati S, Quadri M, Fang M, Rood JP, Saute JA, Chien HF, et al. DNAJC6 mutations associated with early-onset Parkinson's disease. Ann Neurol. 2016;79:244–56.
13. Chang D, Nalls MA, Hallgrímsdóttir IB, Hunkapiller J, van der Brug M, Cai F, et al. A meta-analysis of genome-wide association studies identifies 17 new Parkinson's disease risk loci. Nat Genet. 2017;49:1511–6.
14. Boulakirba S, Macia E, Partisani M, Lacas-Gervais S, Brau F, Luton F, et al. Arf6 exchange factor EFA6 and endophilin directly interact at the plasma membrane to control clathrin-mediated endocytosis. Proc Natl Acad Sci U S A. 2014;111:9473–8.
15. Cao M, Park D, Wu Y, De Camilli P. Absence of Sac2/INPP5F enhances the phenotype of a Parkinson's disease mutation of synaptojanin 1. Proc Natl Acad Sci U S A. 2020;117:12428–34.
16. Yim YI, Sun T, Wu LG, Raimondi A, De Camilli P, Eisenberg E, et al. Endocytosis and clathrin-uncoating defects at synapses of auxilin knockout mice. Proc Natl Acad Sci U S A. 2010;107:4412–7.
17. Conner SD, Schmid SL. Regulated portals of entry into the cell. Nature. 2003;422:37–44.
18. Saheki Y, De Camilli P. Synaptic vesicle endocytosis. Cold Spring Harb Perspect Biol. 2012;4:a005645.

19. Garcia-Alai MM, Heidemann J, Skruzny M, Gieras A, Mertens HDT, Svergun DI, et al. Epsin and Sla2 form assemblies through phospholipid interfaces. Nat Commun. 2018;9:328.
20. Helbig I, Lopez-Hernandez T, Shor O, Galer P, Ganesan S, Pendziwiat M, et al. A recurrent missense variant in AP2M1 impairs clathrin-mediated endocytosis and causes developmental and epileptic encephalopathy. Am J Hum Genet. 2019;104:1060–72.
21. Mao Y, Chen J, Maynard JA, Zhang B, Quiocho FA. A novel all helix fold of the AP180 amino-terminal domain for phosphoinositide binding and clathrin assembly in synaptic vesicle endocytosis. Cell. 2001;104:433–40.
22. He K, Marsland R III, Upadhyayula S, Song E, Dang S, Capraro BR, et al. Dynamics of phosphoinositide conversion in clathrin-mediated endocytic traffic. Nature. 2017;552:410–4.
23. Mim C, Cui H, Gawronski-Salerno JA, Frost A, Lyman E, Voth GA, et al. Structural basis of membrane bending by the N-BAR protein endophilin. Cell. 2012;149:137–45.
24. McMahon HT, Boucrot E. Molecular mechanism and physiological functions of clathrin-mediated endocytosis. Nat Rev Mol Cell Biol. 2011;12:517–33.
25. Rosendale M, Van TNN, Grillo-Bosch D, Sposini S, Claverie L, Gauthereau I, et al. Functional recruitment of dynamin requires multimeric interactions for efficient endocytosis. Nat Commun. 2019;10:4462.
26. Daumke O, Roux A, Haucke V. BAR domain scaffolds in dynamin-mediated membrane fission. Cell. 2014;156:882–92.
27. Hohendahl A, Talledge N, Galli V, Shen PS, Humbert F, De Camilli P, et al. Structural inhibition of dynamin-mediated membrane fission by endophilin. Elife. 2017;6:e26856.
28. Cao M, Wu Y, Ashrafi G, McCartney AJ, Wheeler H, Bushong EA, et al. Parkinson Sac domain mutation in synaptojanin 1 impairs clathrin uncoating at synapses and triggers dystrophic changes in dopaminergic axons. Neuron. 2017;93:882 – 96.e5..
29. Chang-Ileto B, Frere SG, Chan RB, Voronov SV, Roux A, Di Paolo G. Synaptojanin 1-mediated PI(4,5)P2 hydrolysis is modulated by membrane curvature and facilitates membrane fission. Dev Cell. 2011;20:206–18.
30. Nguyen M, Krainc D. LRRK2 phosphorylation of auxilin mediates synaptic defects in dopaminergic neurons from patients with Parkinson's disease. Proc Natl Acad Sci U S A. 2018;115:5576–81.
31. Chen Y, Yong J, Martínez-Sánchez A, Yang Y, Wu Y, De Camilli P, et al. Dynamic instability of clathrin assembly provides proofreading control for endocytosis. J Cell Biol. 2019;218:3200–11.
32. Kaksonen M, Roux A. Mechanisms of clathrin-mediated endocytosis. Nat Rev Mol Cell Biol. 2018;19:313–26.
33. Pranke IM, Morello V, Bigay J, Gibson K, Verbavatz JM, Antonny B, et al. α-Synuclein and ALPS motifs are membrane curvature sensors whose contrasting chemistry mediates selective vesicle binding. J Cell Biol. 2011;194:89–103.

34. Eguchi K, Taoufiq Z, Thorn-Seshold O, Trauner D, Hasegawa M, Takahashi T. Wild-type monomeric α-synuclein can impair vesicle endocytosis and synaptic fidelity via tubulin polymerization at the calyx of held. J Neurosci. 2017;37:6043–52.
35. Medeiros AT, Soll LG, Tessari I, Bubacco L, Morgan JR. α-Synuclein dimers impair vesicle fission during clathrin-mediated synaptic vesicle recycling. Front Cell Neurosci. 2017;11:388.
36. Schechter M, Atias M, Abd Elhadi S, Davidi D, Gitler D, Sharon R. α-Synuclein facilitates endocytosis by elevating the steady-state levels of phosphatidylinositol 4,5-bisphosphate. J Biol Chem. 2020;295:18076–90.
37. Jost M, Simpson F, Kavran JM, Lemmon MA, Schmid SL. Phosphatidylinositol-4,5-bisphosphate is required for endocytic coated vesicle formation. Curr Biol. 1998;8:1399–402.
38. Zoncu R, Perera RM, Sebastian R, Nakatsu F, Chen H, Balla T, et al. Loss of endocytic clathrin-coated pits upon acute depletion of phosphatidylinositol 4,5-bisphosphate. Proc Natl Acad Sci U S A. 2007;104:3793–8.
39. Yoon Y, Zhang X, Cho W. Phosphatidylinositol 4,5-bisphosphate (PtdIns(4,5)P2) specifically induces membrane penetration and deformation by Bin/amphiphysin/Rvs (BAR) domains. J Biol Chem. 2012;287:34078–90.
40. Daste F, Walrant A, Holst MR, Gadsby JR, Mason J, Lee JE, et al. Control of actin polymerization via the coincidence of phosphoinositides and high membrane curvature. J Cell Biol. 2017;216:3745–65.
41. Di Paolo G, De Camilli P. Phosphoinositides in cell regulation and membrane dynamics. Nature. 2006;443:651–7.
42. Voronov SV, Frere SG, Giovedi S, Pollina EA, Borel C, Zhang H, et al. Synaptojanin 1-linked phosphoinositide dyshomeostasis and cognitive deficits in mouse models of Down's syndrome. Proc Natl Acad Sci U S A. 2008;105:9415–20.
43. Hansen C, Björklund T, Petit GH, Lundblad M, Murmu RP, Brundin P, et al. A novel α-synuclein-GFP mouse model displays progressive motor impairment, olfactory dysfunction and accumulation of α-synuclein-GFP. Neurobiol Dis. 2013;56:145–55.
44. Zou L, Zhang X, Xiong M, Meng L, Tian Y, Pan L, et al. Asparagine endopeptidase cleaves synaptojanin 1 and triggers synaptic dysfunction in Parkinson's disease. Neurobiol Dis. 2021;154:105326.
45. Murmu RP, Li W, Holtmaat A, Li JY. Dendritic spine instability leads to progressive neocortical spine loss in a mouse model of Huntington's disease. J Neurosci. 2013;33:12997–3009.
46. Banks SML, Medeiros AT, McQuillan M, Busch DJ, Ibarraran-Viniegra AS, Sousa R, et al. Hsc70 ameliorates the vesicle recycling defects caused by excess α-synuclein at synapses. eNeuro. 2020;7:0448.
47. Busch DJ, Oliphint PA, Walsh RB, Banks SM, Woods WS, George JM, et al. Acute increase of α-synuclein inhibits synaptic vesicle recycling evoked during intense stimulation. Mol Biol Cell. 2014;25:3926–41.

48. Morgan JR, Di Paolo G, Werner H, Shchedrina VA, Pypaert M, Pieribone VA, et al. A role for talin in presynaptic function. J Cell Biol. 2004;167:43–50.
49. Elabi O, Gaceb A, Carlsson R, Padel T, Soylu-Kucharz R, Cortijo I, et al. Human α-synuclein overexpression in a mouse model of Parkinson's disease leads to vascular pathology, blood brain barrier leakage and pericyte activation. Sci Rep. 2021;11:1120.
50. Giasson BI, Duda JE, Quinn SM, Zhang B, Trojanowski JQ, Lee VM. Neuronal alpha-synucleinopathy with severe movement disorder in mice expressing A53T human alpha-synuclein. Neuron. 2002;34:521–33.
51. Taylor TN, Potgieter D, Anwar S, Senior SL, Janezic S, Threlfell S, et al. Region-specific deficits in dopamine, but not norepinephrine, signaling in a novel A30P α-synuclein BAC transgenic mouse. Neurobiol Dis. 2014;62:193–207.
52. Chesselet MF, Richter F. Modelling of Parkinson's disease in mice. Lancet Neurol. 2011;10:1108–18.
53. Nemani VM, Lu W, Berge V, Nakamura K, Onoa B, Lee MK, et al. Increased expression of alpha-synuclein reduces neurotransmitter release by inhibiting synaptic vesicle reclustering after endocytosis. Neuron. 2010;65:66–79.
54. Xu J, Wu XS, Sheng J, Zhang Z, Yue HY, Sun L, et al. α-Synuclein mutation inhibits endocytosis at mammalian central nerve terminals. J Neurosci. 2016;36:4408–14.
55. Lu J, Sun F, Ma H, Qing H, Deng Y. Comparison between α-synuclein wild-type and A53T mutation in a progressive Parkinson's disease model. Biochem Biophys Res Commun. 2015;464:988–93.
56. Conway KA, Lee SJ, Rochet JC, Ding TT, Williamson RE, Lansbury PT Jr. Acceleration of oligomerization, not fibrillization, is a shared property of both alpha-synuclein mutations linked to early-onset Parkinson's disease: implications for pathogenesis and therapy. Proc Natl Acad Sci U S A. 2000;97:571–6.
57. Coskuner O, Wise-Scira O. Structures and free energy landscapes of the A53T mutant-type α-synuclein protein and impact of A53T mutation on the structures of the wild-type α-synuclein protein with dynamics. ACS Chem Neurosci. 2013;4:1101–13.
58. Uversky VN, Li J, Fink AL. Evidence for a partially folded intermediate in alpha-synuclein fibril formation. J Biol Chem. 2001;276:10737–44.
59. Martin LJ, Pan Y, Price AC, Sterling W, Copeland NG, Jenkins NA, et al. Parkinson's disease alpha-synuclein transgenic mice develop neuronal mitochondrial degeneration and cell death. J Neurosci. 2006;26:41–50.
60. Ingelsson M. Alpha-synuclein oligomers-neurotoxic molecules in Parkinson's disease and other Lewy body disorders. Front Neurosci. 2016;10:408.
61. Cuervo AM, Stefanis L, Fredenburg R, Lansbury PT, Sulzer D. Impaired degradation of mutant alpha-synuclein by chaperone-mediated autophagy. Science. 2004;305:1292–5.
62. Moretti P, Mariani P, Ortore MG, Plotegher N, Bubacco L, Beltramini M, et al. Comprehensive structural and thermodynamic analysis of prefibrillar WT α-synuclein and its G51D, E46K, and A53T mutants by

a combination of small-angle X-ray scattering and variational bayesian weighting. J Chem Inf Model. 2020;60:5265–81.

63. Zanazzi G, Matthews G. A doubleheader in endocytosis. Neuron. 2007;56:939–42.
64. Cremona O, Di Paolo G, Wenk MR, Lüthi A, Kim WT, Takei K, et al. Essential role of phosphoinositide metabolism in synaptic vesicle recycling. Cell. 1999;99:179–88.
65. Harris TW, Hartwieg E, Horvitz HR, Jorgensen EM. Mutations in synaptojanin disrupt synaptic vesicle recycling. J Cell Biol. 2000;150:589–600.
66. Verstreken P, Koh TW, Schulze KL, Zhai RG, Hiesinger PR, Zhou Y, et al. Synaptojanin is recruited by endophilin to promote synaptic vesicle uncoating. Neuron. 2003;40:733–48.
67. Mettlen M, Chen PH, Srinivasan S, Danuser G, Schmid SL. Regulation of clathrin-mediated endocytosis. Annu Rev Biochem. 2018;87:871–96.
68. Koo SJ, Markovic S, Puchkov D, Mahrenholz CC, Beceren-Braun F, Maritzen T, et al. SNARE motif-mediated sorting of synaptobrevin by the endocytic adaptors clathrin assembly lymphoid myeloid leukemia (CALM) and AP180 at synapses. Proc Natl Acad Sci U S A. 2011;108:13540–5.

Figures

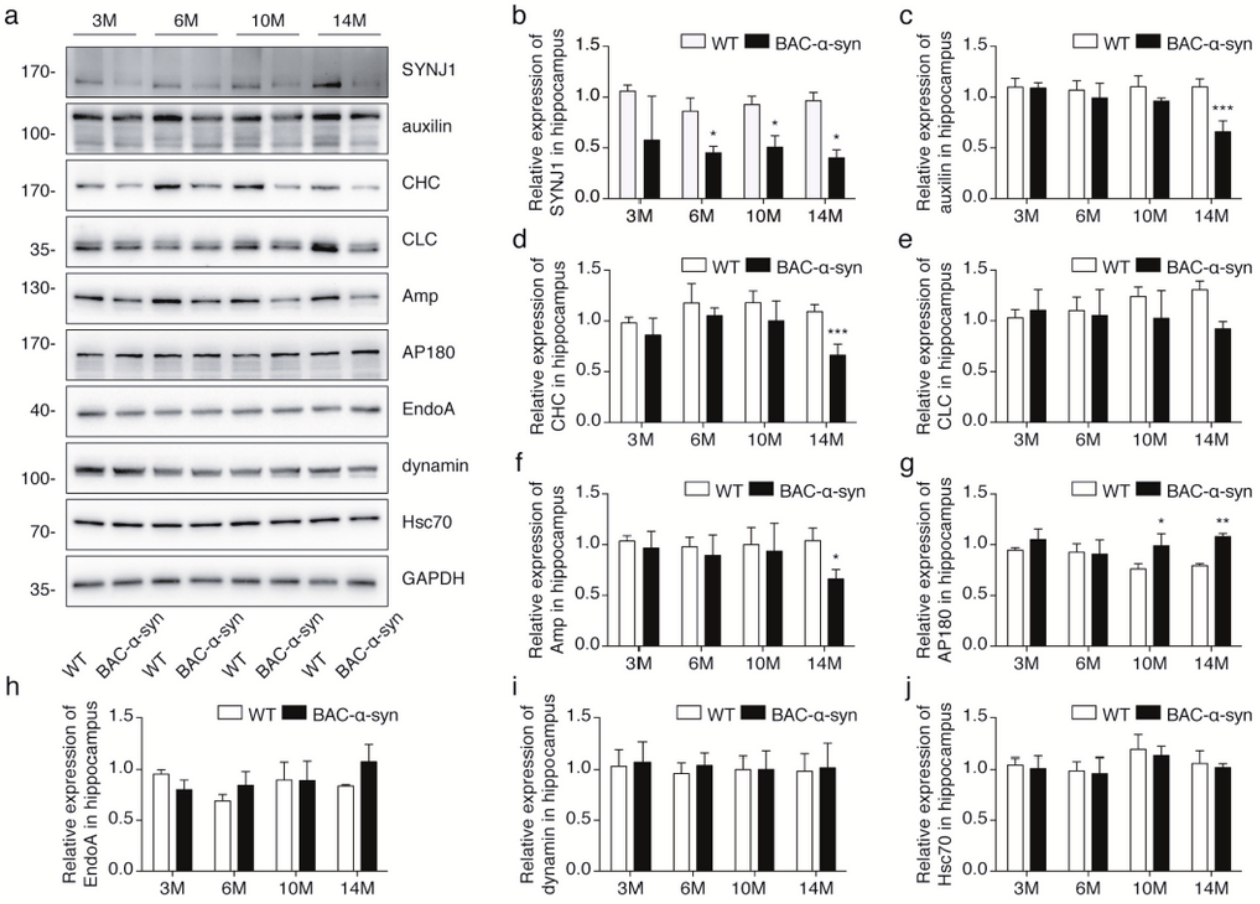

Figure 1

CME-associated proteins in the hippocampus of BAC-α-syn mice.

(a) Western blot showing the amounts of a variety of CME-associated proteins in the hippocampus of 3-, 6-, 10- and 14-month-old BAC-α-syn and WT mice. (b-j) Quantification of relative protein levels of SYNJ1 (b), auxilin (c), CHC (d), CLC(e), Amp (f), AP180 (g), EndoA (h), dynamin (i) and Hsc70 (j) from at least three independent pairs of samples. Two-way ANOVA with Tukey's post hoc test. *$p < 0.05$, **$p < 0.01$, ***$p < 0.001$, ****$p < 0.0001$were considered to be significant.

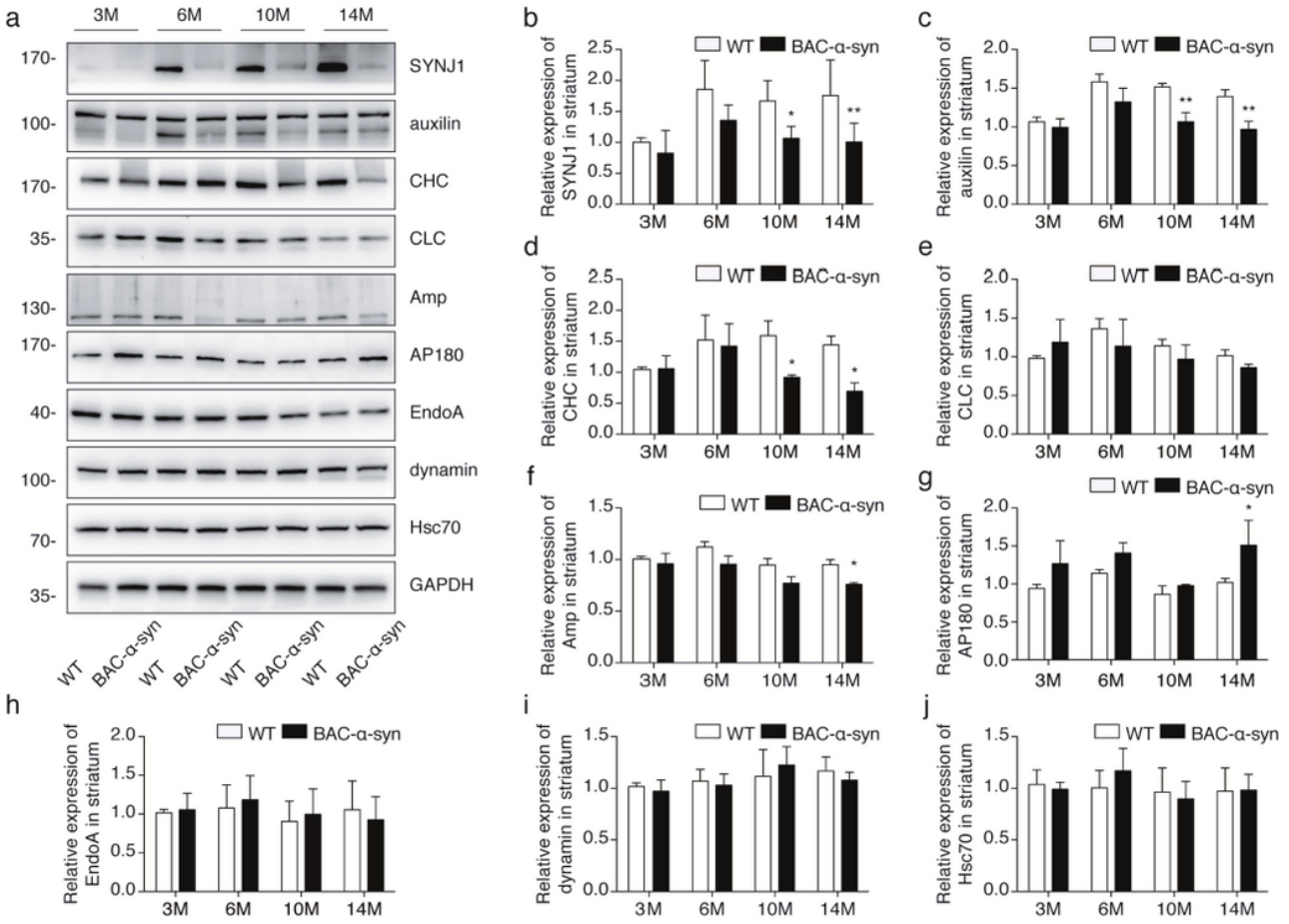

Figure 2

CME-associated proteins in the striatum of BAC-α-syn mice.

(a) Western blot showing the amounts of a variety of CME-associated proteins in the striatum of 3-, 6-, 10- and 14-month-old BAC-α-syn and WT mice. (b-j) Quantification of relative protein levels of SYNJ1 (b),

auxilin (c), CHC (d), CLC(e), Amp (f), AP180 (g), EndoA (h), dynamin (i) and Hsc70 (j) from at least three independent pairs of samples. Two-way ANOVA with Tukey's post hoc test. *$p < 0.05$, **$p < 0.01$, ***$p < 0.001$, ****$p < 0.0001$ were considered to be significant.

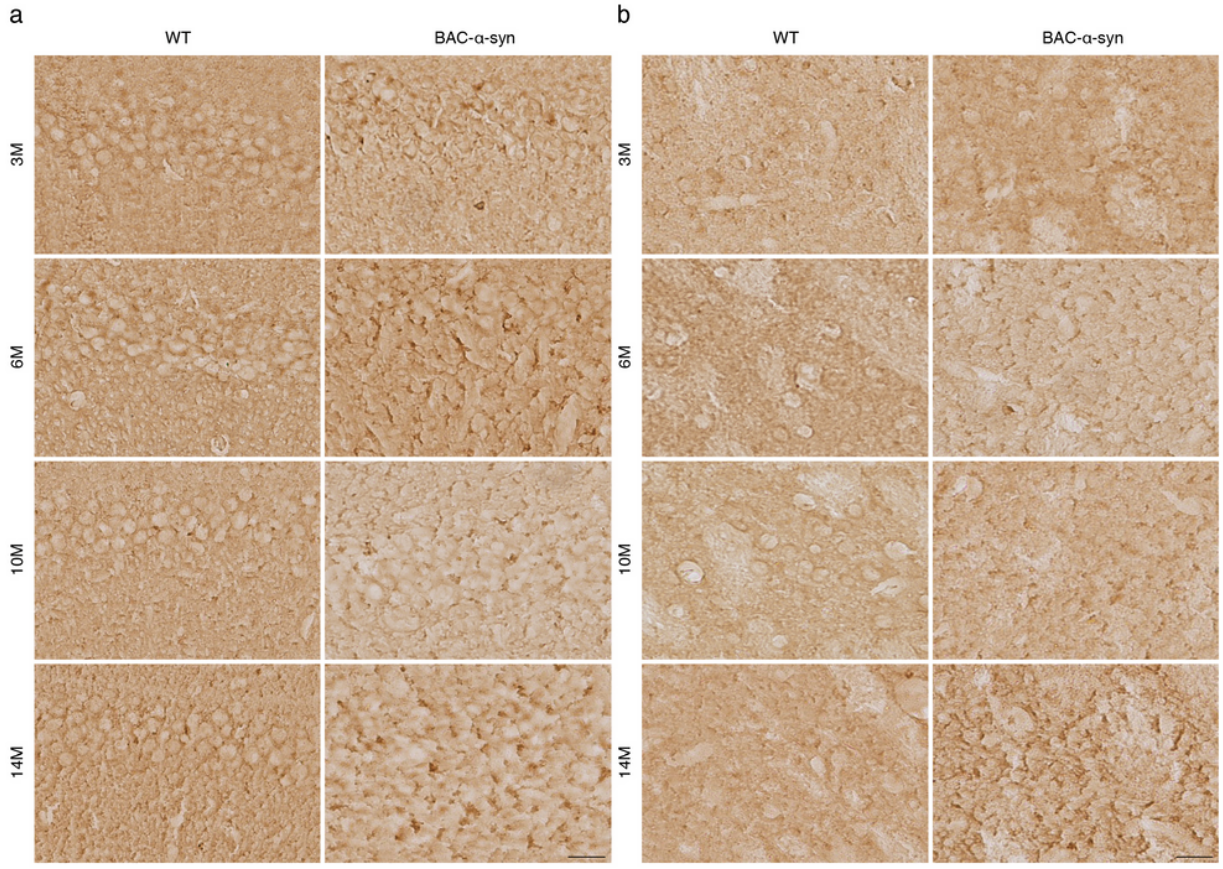

Figure 3

Clustering of SYNJ1 in BAC-α-syn mice.

(a) Immunohistochemistry for SYNJ1 in the hippocampus of 3-, 6-, 10- and 14-month-old BAC-α-syn and WT mice show clustering of SYNJ1 from 6 month. Scale bar, 20μm. (b) Immunohistochemistry for SYNJ1 in the striatum of 3-, 6-, 10- and 14-month-old BAC-α-syn and WT mice show clustering of SYNJ1 from 6 month. Scale bar, 20μm.

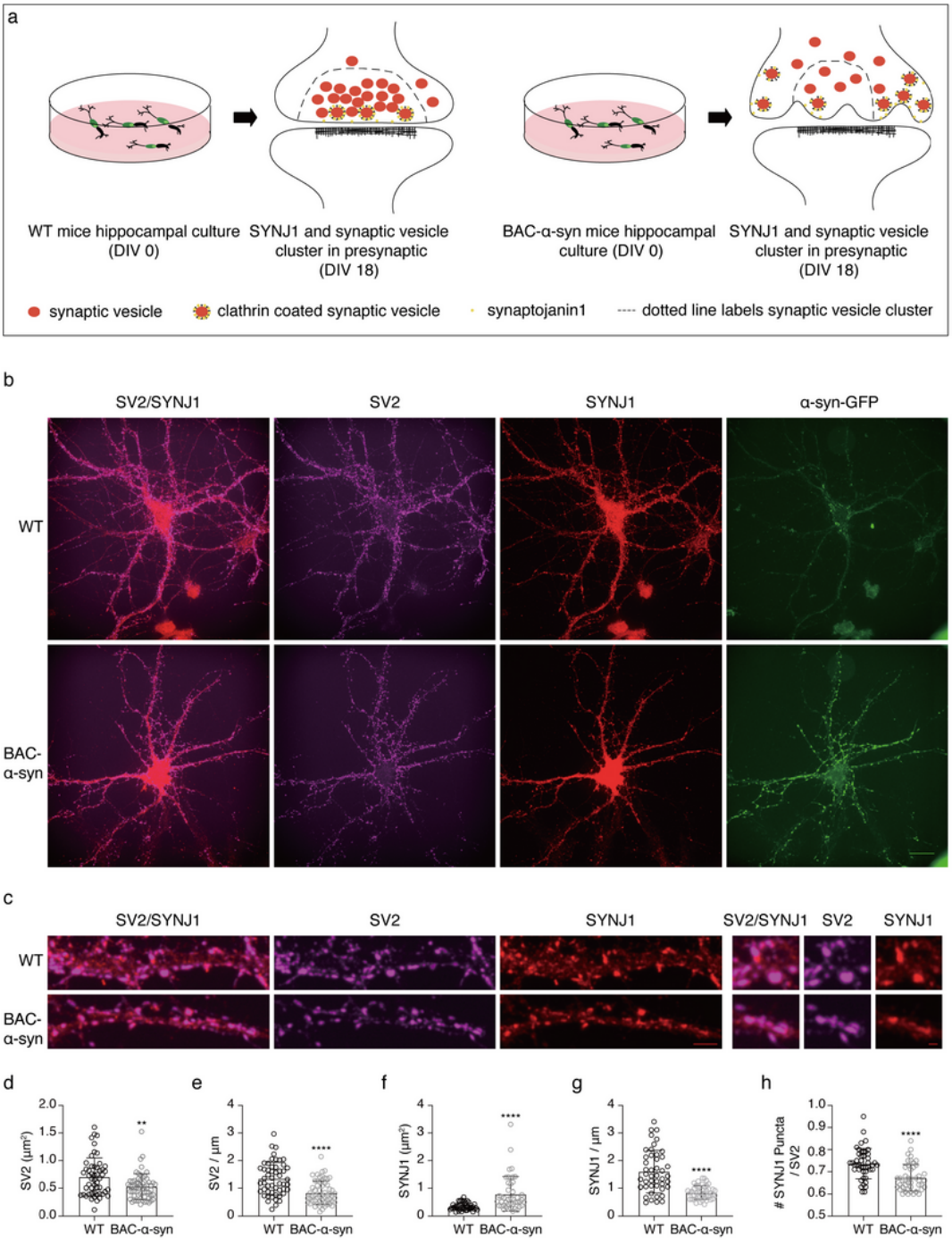

Figure 4

Overexpression of α-syn reduces and clusters SYNJ1 at presynaptic in primary neurons.

(a) Experimental timeline paradigm of the primary neuron experiment, the area circled by dotted line indicates synaptic vesicle cluster, which is labeled by SV2 antibody, and yellow circle indicates SYNJ1. (b) Immunostaining of SV2 and SYNJ1 of DIV18 primary neurons from BAC-α-syn and WT mice. Purple

indicates SV2, red indicates SYNJ1 and green indicates α-syn-GFP. Scale bar, 20μm. (c) Dendritic segments of the figure (b). Dendrite enlarge picture, scale bar, 100μm. Positive puncta enlarge picture, scale bar, 200μm. (d-g) Quantifications of the puncta area and the linear density of SV2 and SYNJ1 clusters. (h) Graphs showing the average number of SYNJ1 puncta per SV2. n = 45-50 dendrites which were derived from 15 neurons obtained from 3 × technical replicates for each mice (5 neurons each mice). Unpaired *t*-test. **p* < 0.05; ***p* < 0.01, ****p* < 0.001, *****p* < 0.0001 were considered to be significant.

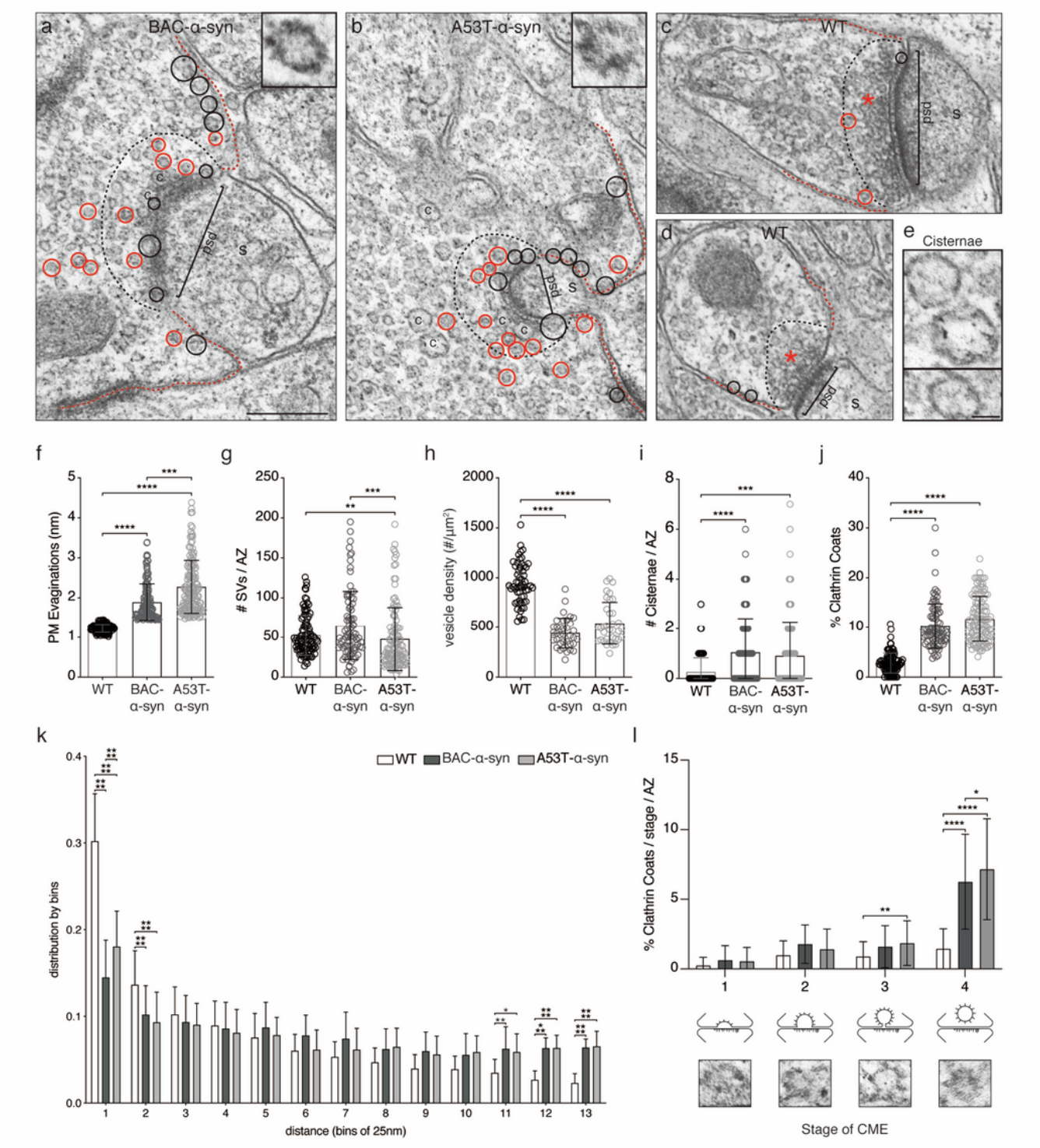

Figure 5

Overexpression of WT-α-syn and A53T-α-syn impairs synaptic vesicle recycling.

(a-d) Electron micrographs from CA1 of hippocampal region in BAC-α-syn (a), α-syn-A53T (b), and WT (c, d) mice. Red asterisks and Black dotted lines mark the clustered vesicles. Red dotted lines indicates the plasma membrane. Black circles means the CCP. Red circles means the CCV. C, cisternae; S, dendritic spine; psd, postsynaptic density. Scale bar, 200 nm. (e) Examples of cisternae in BAC-α-syn and α-syn-A53T mice. Scale bar, 50 nm. (f) In contrast to WT mice, BAC-α-syn and α-syn-A53T mice show a buildup of PM. (g) The total synaptic vesicles in the active zone only increase in α-syn-A53T mice. (h) Clustered vesicles in BAC-α-syn, α-syn-A53T mice significantly reduced compared to the WT mice. (i) The number of large cisternae were increased in BAC-α-syn and α-syn-A53T mice. (j) The increase in clathrin coated vesicles in BAC-α-syn and α-syn-A53T mice indicates defects of recycling vesicles. (k) Histogram with bins indicating the distances from the active zone: 1:25-50 nm, 2:50-75 nm, 3:75-100 nm, 4:100-125 nm, 5:125-150 nm, 6:150-175 nm, 7:175-200 nm, 8:200-225 nm, 9:225-250 nm, 10:250-275 nm, 11:275-300 nm, 12:300-325 nm, 13:325-350 nm. (l) Quantitative analysis of each morphologically distinct stage of CCP and CCV formation. This analysis revealed vesicle fission defected only in α-syn-A53T mice, as indicated by a selective increase in stage 3 CCPs. In addition, clathrin uncoating defected both in BAC-α-syn and α-syn-A53T mice (stage 4). Bars represent mean SD from n = 70-100 synapses, 3 mice. One way ANOVA (f-j), Two-way ANOVA with Tukey's post hoc test (k, l). *$p < 0.05$, **$p < 0.01$, ***$p < 0.001$, ****$p < 0.0001$ were considered to be significant.

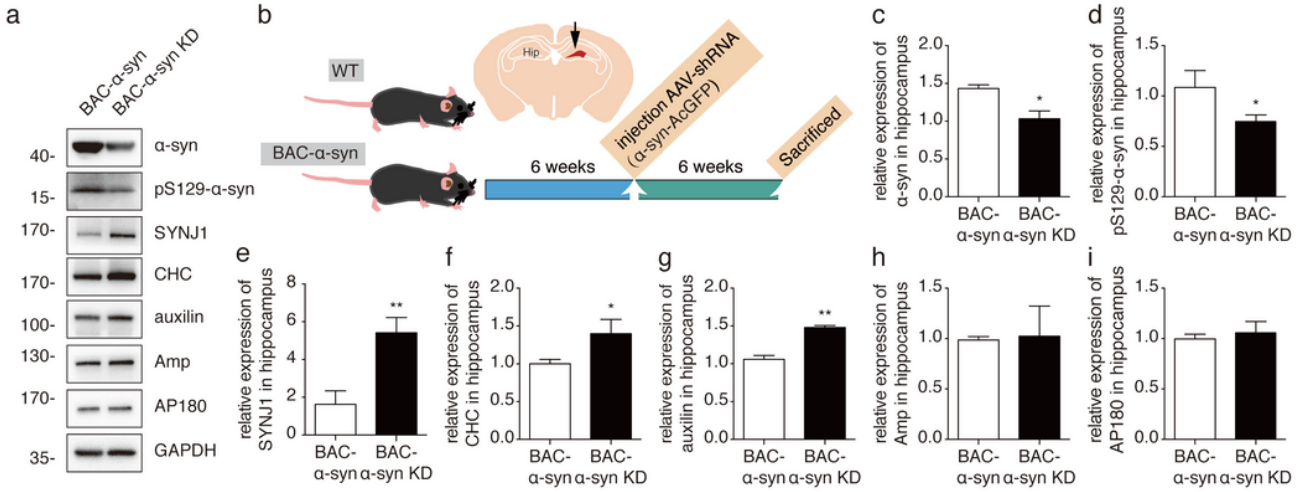

Figure 6

α-Syn knockdown restores the CME-associated proteins expression in the hippocampus of BAC-α-syn mice.

(a) Western blot analysis of abnormal α-syn and CME-associated proteins of the hippocampus from the injection side and contralateral side of the injection of BAC-α-syn mice, 6 weeks after AAV vector delivery. (b) Experimental timeline paradigm of unilaterally injected AAV-shRNA (α-syn-AcGFP) into the DG of WT and BAC-α-syn mice. (c-d) The expression levels of α-syn (c) and phosphorylated α-syn (d) reduced in AAV-shRNA (α-syn-AcGFP) injected side. (e-i) Quantification of expression levels of other CME-associated proteins. SYNJ1 (e), CHC (f), auxilin (g), Amp (h), AP180 (i). n = 3. Unpaired *t*-test. *$p < 0.05$; **$p < 0.01$, ***$p < 0.001$, ****$p < 0.0001$ were considered to be significant.

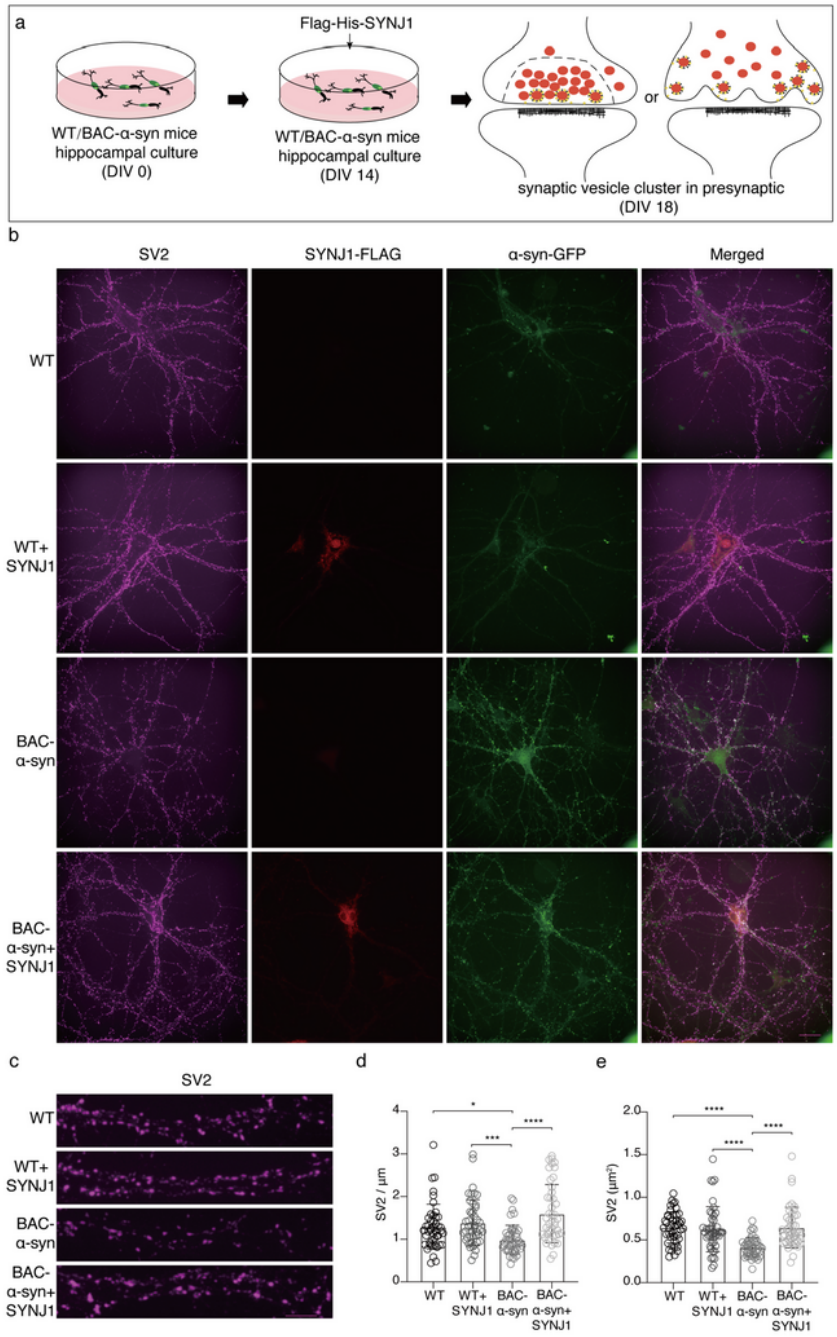

Figure 7

Exogenous SYNJ1 restores the level of synaptic vesicle cluster reduced by α-syn

(a) Experimental timeline paradigm of the primary neurons transfected with Flag-His-tagged SYNJ1. (b) Immunostaining of SV2 of DIV18 primary neurons transfected with Flag-His-tagged SYNJ1 of both BAC-α-syn and WT mice, and the corresponding control group. Purple indicates SV2, red indicates Flag-His-tagged SYNJ1 and green indicates α-syn-GFP. Scale bar, 20μm. (c) Dendritic segments of the figure (b). Scale bar, 100μm. (d-e) Quantifications of the linear density and the puncta area of SV2 clusters. n = 45-50 dendrites which were derived from 15 neurons obtained from 3 × technical replicates for each mice (5 neurons each mice). One way ANOVA. *$p < 0.05$, **$p < 0.01$, ***$p < 0.001$, ****$p < 0.0001$ were considered to be significant.

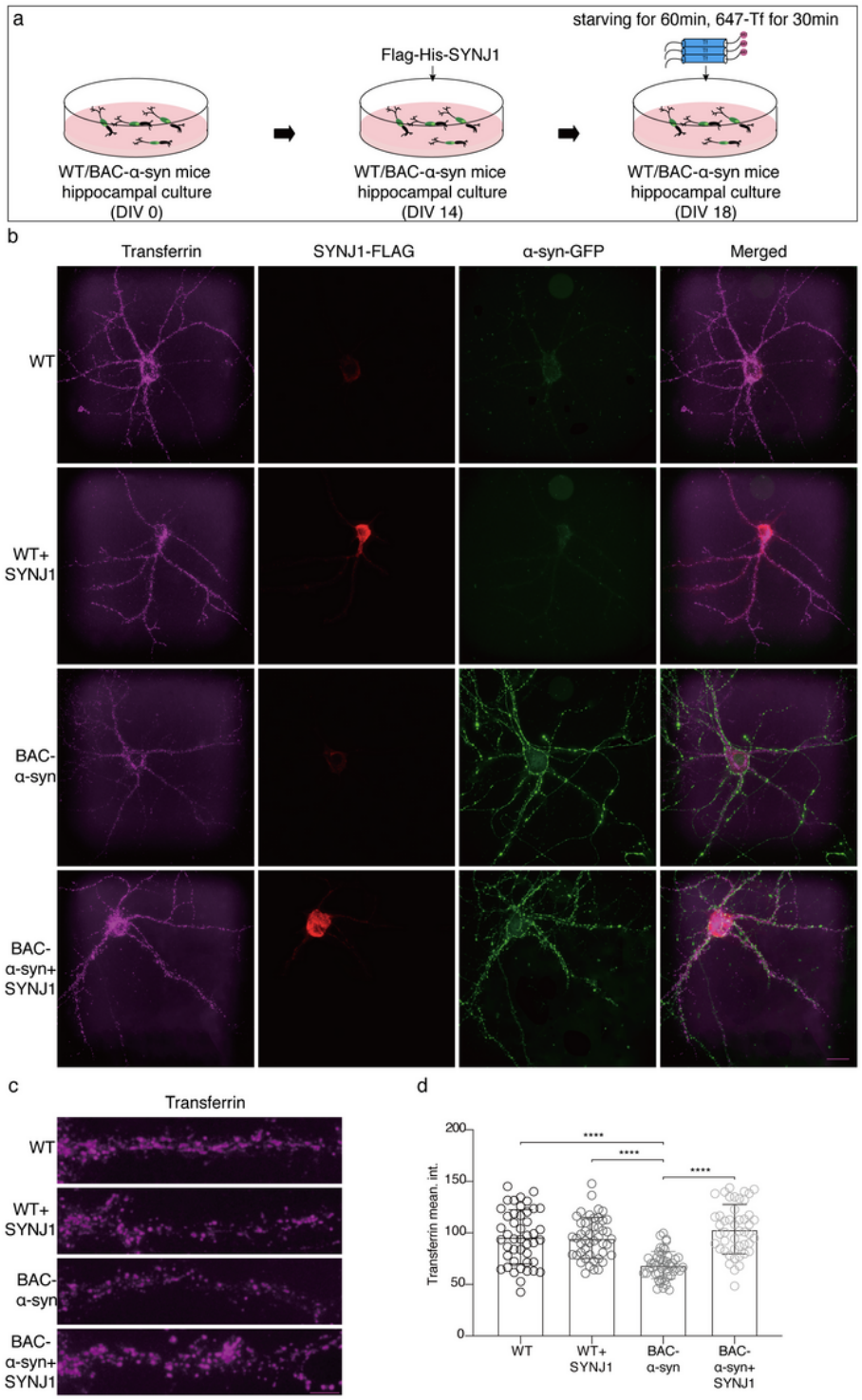

Figure 8

Exogenous SYNJ1 reverses the α-syn-induced CME dysfunction.

(a) Experimental timeline paradigm of the primary neurons added with 647-Tf. (b) Transferrin uptake assay. DIV14 primary neurons transfected with Flag-His-tagged SYNJ1 of both BAC-α-syn and WT mice, four days later, neurons were incubated in parallel with 647-Tf at 37 ◦C for 30 min. Purple indicates

transferrin, red indicates Flag-His-tagged SYNJ1 and green indicates α-syn-GFP. Scale bar, 20μm. (c) Dendritic segments of the figure (b). Scale bar, 100μm. (d) Quantifications of the mean fluorescence intensity of transferrin. n = 45-50 dendrites which were derived from 15 neurons obtained from 3 × technical replicates for each mice (5 neurons each mice). One way ANOVA. *$p < 0.05$, **$p < 0.01$, ***$p < 0.001$, ****$p < 0.0001$ were considered to be significant.

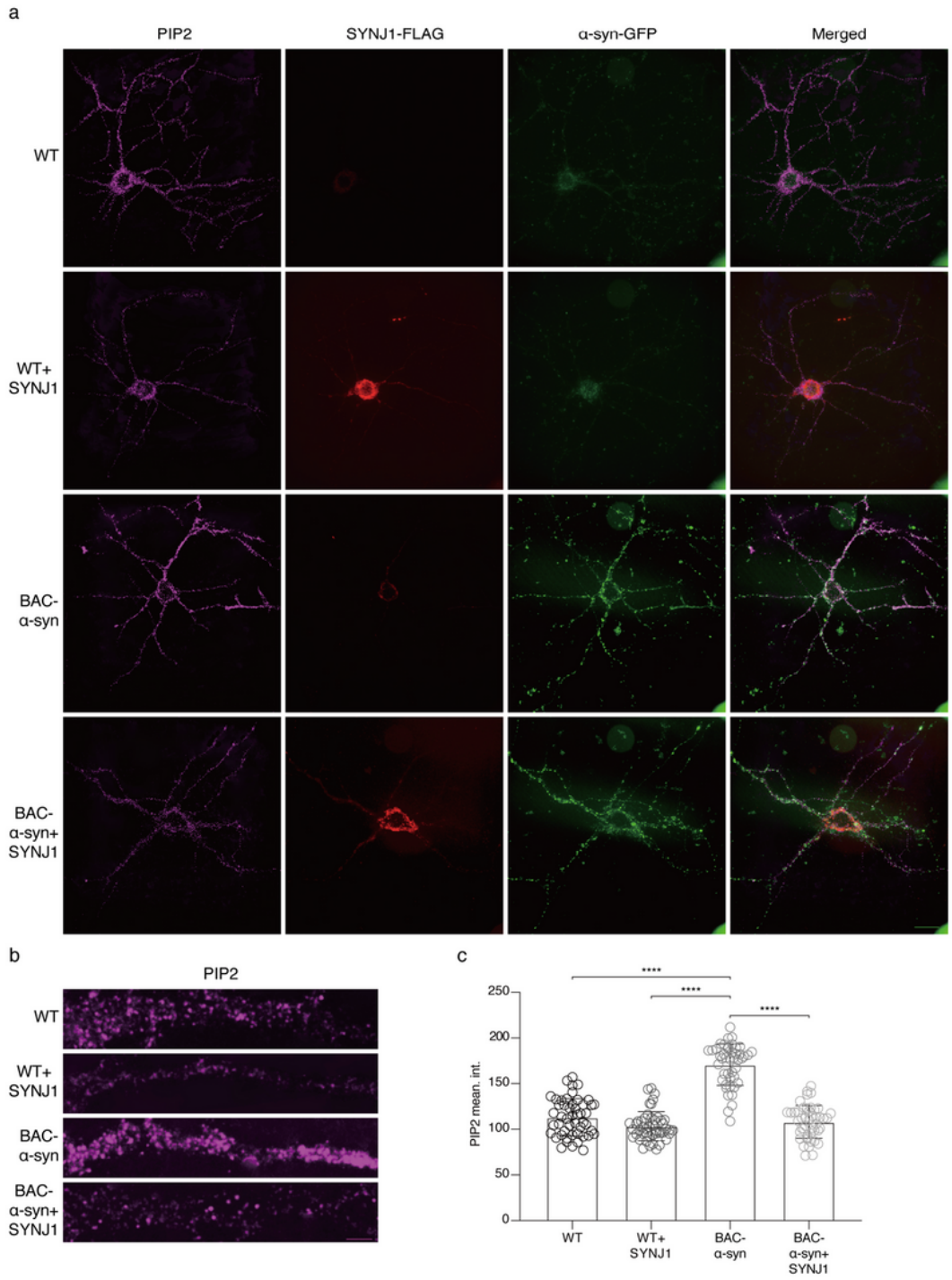

Figure 9

SYNJ1 attenuates the CME defects caused by α-syn through $PI(4,5)P_2$

(a) Immunostaining of PIP2 of the DIV18 primary neurons transfected with Flag-His-tagged SYNJ1 of both BAC-α-syn and WT mice, and the corresponding control group. Purple indicates PIP2, red indicates Flag-His-tagged SYNJ1 and green indicates α-syn-GFP. Scale bar, 20μm. (b) Dendritic segments of the figure (a). Scale bar, 100μm. (c) Quantifications of the mean fluorescence intensity of PIP2. n = 45-50 dendrites which were derived from 15 neurons obtained from 3 × technical replicates for each mice (5 neurons each mice). One way ANOVA. *$p < 0.05$, **$p < 0.01$, ***$p < 0.001$, ****$p < 0.0001$ were considered to be significant.

Supplementary Files

This is a list of supplementary files associated with this preprint. Click to download.

- Additionalfile1.pdf